NEUROSCIENCE

BBB opening with focused ultrasound in nonhuman primates and Parkinson's disease patients: Targeted AAV vector delivery and PET imaging

Javier Blesa[1,2]†, José A. Pineda-Pardo[1,2]†, Ken-ichi Inoue[3], Carmen Gasca-Salas[1,2,4], Tiziano Balzano[1], Natalia López-González Del Rey[1,5], Alejandro Reinares-Sebastián[1], Noelia Esteban-García[1,5], Rafael Rodríguez-Rojas[1,2], Raquel Márquez[1], María Ciorraga[1], Marta del Álamo[1], Lina García-Cañamaque[4,6], Santiago Ruiz de Aguiar[7], Itay Rachmilevitch[8], Inés Trigo-Damas[1,2], Masahiko Takada[3,9], José A. Obeso[1,2,4]*

Intracerebral vector delivery in nonhuman primates has been a major challenge. We report successful blood-brain barrier opening and focal delivery of adeno-associated virus serotype 9 vectors into brain regions involved in Parkinson's disease using low-intensity focus ultrasound in adult macaque monkeys. Openings were well tolerated with generally no associated abnormal magnetic resonance imaging signals. Neuronal green fluorescent protein expression was observed specifically in regions with confirmed blood-brain barrier opening. Similar blood-brain barrier openings were safely demonstrated in three patients with Parkinson's disease. In these patients and in one monkey, blood-brain barrier opening was followed by ^{18}F-Choline uptake in the putamen and midbrain regions based on positron emission tomography. This indicates focal and cellular binding of molecules that otherwise would not enter the brain parenchyma. The less-invasive nature of this methodology could facilitate focal viral vector delivery for gene therapy and might allow early and repeated interventions to treat neurodegenerative disorders.

INTRODUCTION

Neurodegenerative disorders such as Parkinson's disease (PD), Alzheimer's disease (AD), Huntington disease (HD), and amyotrophic lateral sclerosis are an increasing worldwide challenge (*1*). There is no cure for any of these neurodegenerative diseases, nor is a therapy currently available to stop or slow down their progression. Potentially promising therapies (i.e., immunotherapy and gene therapy) are often limited by their inability to cross efficiently the blood-brain barrier (BBB), a naturally occurring system that can drastically reduce the diffusion of drugs and toxins into the central nervous system (*2*). Thus, establishing disease-modifying strategies and overcoming difficulties in efficient intracerebral drug administration are a potential major therapeutic development against neurodegenerative diseases (*3*).

Gene therapy has the potential to provide an important benefit through several means, including correction of pathogenic mechanisms, neuroprotection, and neurorestoration (*4*). Adeno-associated virus (AAV) vectors have emerged particularly as an attractive vehicle for gene transfer (*5*). To target focal brain structures, however, therapeutic genetic trials currently require direct intrathecal or intracerebral injections, which is a critical factor limiting the use of AAV vectors. In addition, neurodegenerative disease treatments may require gene (or other molecules) delivery into several brain regions simultaneously (*6*). Therefore, an ideal gene delivery approach to brain diseases should be safe, noninvasive, and region specific. However, systemic viral vector administration is hampered by the inability to reach a specific or exclusive target focally in the brain (*7*).

Recently, it has been shown that low-intensity focused ultrasound (LIFU) combined with intravenously circulating microbubbles can be applied safely to transiently open the BBB (*8*–*14*). This would allow drug delivery (*15*, *16*) in human patients and successfully enhance intracerebral viral vector delivery in AD, HD, and PD rodent models (*17*, *18*). Efficient BBB opening in nonhuman primates (NHPs) has been achieved previously (*19*–*23*). However, translating rodent findings of systemic viral vector administration to NHPs has been unsuccessful thus far (*24*–*27*). In general, NHPs share enormous anatomical and physiological similarities with humans, for instance, brain structural organization, BBB physiology, and immune response (*28*). Thus, using NHPs to improve and tailor the methodology for safe gene transfer appears to be the best model before embarking on clinical trials in humans (*29*).

Toward this aim, we have evaluated the safety and feasibility of intravenous AAV vector delivery following BBB opening with LIFU targeting the nigrostriatal system and other brain regions relevant to PD in normal and parkinsonian NHPs. Among neurodegenerative disorders, we focus on PD, since early in its evolution, particularly in a non-elderly population, neuronal degeneration is limited to dopaminergic cells in the substantia nigra pars compacta (SNc) and the corresponding dopaminergic fibers in the putamen (*30*,

[1]HM CINAC (Centro Integral de Neurociencias Abarca Campal), Hospital Universitario HM Puerta del Sur, HM Hospitales, Madrid, Spain. [2]Network Center for Biomedical Research on Neurodegenerative Diseases (CIBERNED), Instituto Carlos III, Madrid, Spain. [3]Systems Neuroscience Section, Department of Neuroscience, Primate Research Institute, and Center for the Evolutionary Origins of Human Behavior, Kyoto University; Inuyama, Aichi 484-8506, Japan. [4]University CEU-San Pablo, Madrid, Spain. [5]PhD Program in Neuroscience Autónoma de Madrid University-Cajal Institute, Madrid, Spain. [6]Department of Nuclear Medicine, Hospital Universitario HM Puerta del Sur, HM Hospitales, Madrid, Spain. [7]Medical Management, Hospital Universitario HM Puerta del Sur, HM Hospitales, Madrid, Spain. [8]Insightec Ltd., Haifa, Israel. [9]Department of Neurology, Graduate School of Medicine, Osaka University, Suita, Osaka 565-0871, Japan.
*Corresponding author. Email: jobeso.hmcinac@hmhospitales.com
†These authors contributed equally to this work.

31). This allows visualization of a possible scenario where treatments acting on the dopaminergic nigrostriatal system could be administered very early in disease evolution (*32*). Accordingly, we have also used ^{18}F-Choline positron emission tomography (PET) imaging to demonstrate that the same BBB opening methodology is functionally successful in the putamen and midbrain structures of patients with PD. Together, our results constitute a valuable step toward achieving the goal of providing putative therapies for PD and other neurodegenerative diseases.

RESULTS

Initial BBB openings in NHPs targeting brain regions relevant to PD

Transcranial LIFU with magnetic resonance imaging (MRI) guidance was applied in six monkeys (M1 to M6). Initially, LIFU was performed in two monkeys (M1/M2) to evaluate the safety and feasibility of BBB opening in several brain regions implicated in PD (Fig. 1). Targeted regions included the premotor cortex (PMC; M1; Fig. 1A), posterior ventrolateral thalamic region (M1; Fig. 1B), striatum (the caudate nucleus and putamen; M2; Fig. 1C), and midbrain (the subthalamic nucleus and substantia nigra; M2; Fig. 1D). For these initial interventions, we followed a previously described protocol (*22*) that has shown the feasibility of focal BBB opening in NHPs (for methodological details and related parameters, see Materials and Methods and table S1). Briefly, a small-sized grid of focal targets spanning 2 by 2 or 1 by 2 matrices in a single axial plane with 2-mm isotropic spacing between grid spots was defined, which resulted in target size-dependent opening at volumes of 17 mm^3 (caudate nucleus), 28 mm^3 (putamen), 28 mm^3 (thalamus), 24 mm^3 (midbrain), and 90 mm^3 (PMC). We assessed BBB opening success by comparing T1-weighted images before and after administration of gadolinium (Gd), a compound that does not otherwise cross the BBB. These brain regions were targeted unilaterally, except for bilateral targeting in the striatum (caudate nucleus on one side and putamen on the other) in M2 (Fig. 1C). BBB openings of moderate magnitude were achieved with relative accuracy. Neither BBB disruption nor other MRI abnormalities were observed elsewhere. No abnormal signal was seen on the follow-up susceptibility-weighted images (SWI) (fig. S1). BBB permeability was restored within 24 hours (fig. S2). No neurological/behavioral manifestations were associated with the BBB opening either acutely or during follow-up.

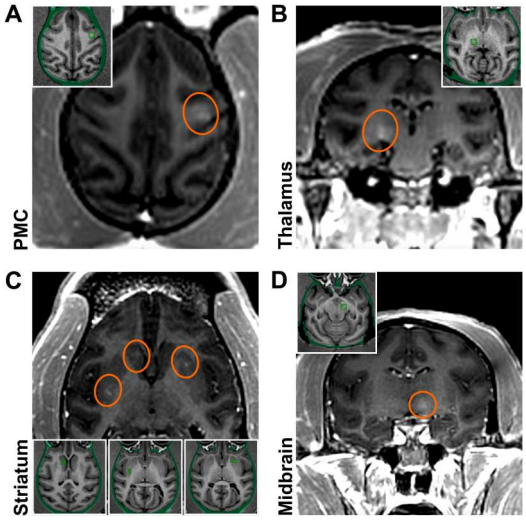

Fig. 1. Initial BBB openings in NHPs targeting brain regions relevant to PD. Successful BBB openings were demonstrated in two monkeys (M1/M2) by delivery of an MR contrast agent (Gd) that does not normally extravasate in the brain. Openings were achieved in the targeted regions with relative accuracy. (**A**) Axial contrast-enhanced T1-weighted MRI image shows BBB disruption in the PMC (indicated by the red circle; M1). (**B**) Coronal contrast-enhanced MRI shows BBB disruption in the posterior ventrolateral thalamic region (M1). (**C**) Axial contrast-enhanced MRI shows BBB disruption in the striatum (both the head of the caudate nucleus and the posterior putamen on one side and the anterior putamen on the other; M2). (**D**) Coronal contrast-enhanced MRI shows BBB disruption in the midbrain (M2). All the enhancements were largely restricted to the targeted regions. Although the same approach was used for each sonication, the size and magnitude of BBB disruption varied depending on the targeted region.

Safe and large-volume BBB openings in the putamen of normal and parkinsonian NHPs by LIFU

Taking therapeutic trials into consideration, a sufficiently large volume BBB opening in the whole putamen is needed, which was carried out in two other animals (M3/M4; Fig. 2) (*32*). The putamen was targeted unilaterally in three axial planes aiming to cover a high proportion of its volume. The effective spacing between spots was reduced from 2 to 1 mm to maximize spatial coverage. Large-

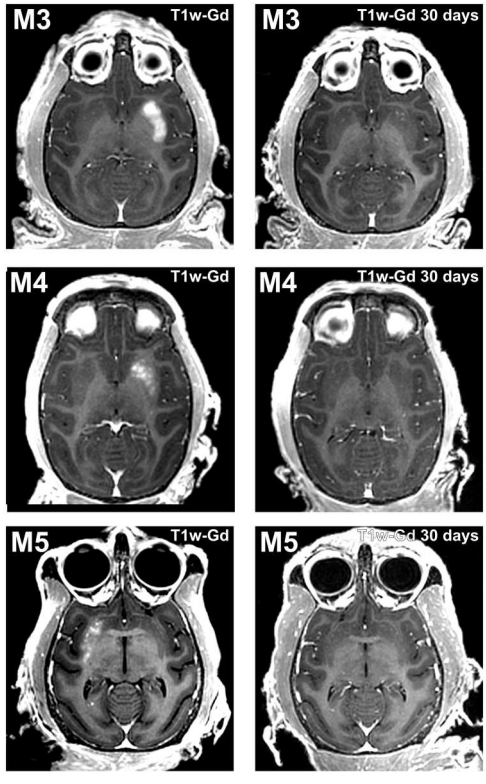

Fig. 2. Safe and large-volume BBB openings in the putamen of normal and parkinsonian NHPs by LIFU. Axial contrast-enhanced T1-weighted images show homogeneous Gd extravasation in the putamen in M3, M4, and parkinsonian monkey M5 immediately after treatment **(left column)** and 30 days later **(right column)**. The areas of enhancement almost perfectly overlapped the targeted regions.

volume BBB openings were observed in the putamena of both monkeys (806 mm^3 and 525 mm^3, respectively), especially in M3 in which the entire region of the putamen was almost covered with Gd as visualized in T1-weighted images (Fig. 2A). The same approach was also conducted in a mildly 1-methyl-4-phenyl-1,2,3,6-tetrahydropyridine (MPTP)–treated monkey (M5) who exhibited ~60% reduction in striatal dopaminergic innervation, as assessed by postmortem immunostaining (fig. S3). This verified the impact of BBB opening on the dopamine-depleted putamen at a volume of 285 mm^3 (Fig. 2C). The experimental procedure was safe for all animals, and BBB opening sessions were well tolerated. Neither neurological nor behavioral deficits were observed after BBB opening in any of the monkeys. Posttreatment SWI, T2-weighted fast spin-echo (T2-FSE), fluid-attenuation inversion recovery (FLAIR), and diffusion-weighted image (DWI) MRIs did not reveal any discernible abnormalities, such as edema, microhemorrhage, or infarction, immediately or 30 days after the opening (Fig. 3). The BBB permeability was reversed within 1 month, although a minor punctate distribution of BBB-opened regions in the anterior putamen was still detected in the monkey (M3) with the largest BBB opening (Fig. 2A).

Delivery of AAV vectors in NHPs

To examine the potential therapeutic value of LIFU BBB openings for gene therapy, the five monkeys (M1 to M5) underwent intravenous administration of AAV serotype 9 (AAV9) vectors expressing green fluorescent protein (GFP) under the control of human synapsin (hSyn) promotor (AAV9-hSyn-GFP). As described in Materials and Methods, two types of modified AAV9-hSyn-GFP vectors, i.e., AAV9-PHPeB and AAV9.2-PHPeB vectors, were used in this study. In intact monkeys (M1 to M4), the AAV9.2-PHPeB vector was injected, while the AAV9-PHPeB vector was injected in a parkinsonian monkey (M5) (for production and injection of these vectors, see Materials and Methods). Neutralizing antibodies (NAbs) against AAV9 were assessed in each animal before the vector administration. Such NAbs recognize and bind to the virus and neutralize it, preventing gene transduction and transgene expression to reduce their efficacy via AAV vectors (*33*–*35*). Four weeks after administration, all the monkeys were euthanized, and the brains were investigated postmortem to evaluate neuronal expression of GFP and other histological markers. The histological analysis revealed successful focal delivery of the modified AAV9-hSyn-GFP vectors that was restricted to the areas of BBB openings (Figs. 4 and (5). In addition, a few neurons were scattered in other non-opened sites as described before (*24*, *35*, *36*). The GFP expression was confirmed not only by immunohistochemistry with two different antibodies but also directly by fluorescent microscopy (native fluorescence) (see fig. S4). This vector-induced GFP expression occurred in three (M2, M3, and M5) of the five monkeys, all of whom were labeled as NAbs free. By contrast, there was no hint of GFP expression in the other two monkeys (M1 and M4) who had NAbs against AAV (Figs. 4J and 5, E and F). Especially in M2, several sites (i.e., the striatal and midbrain regions) were targeted simultaneously and bilaterally (Fig. 4, B and G). Postmortem assessment revealed focal clusters of GFP-positive (GFP^+) neurons in the areas that matched the Gd contrast enhancement observed by MRI and no marked GFP expression in any other areas (Fig. 4, A, C to F, and H to J). The vector delivery yielded 10-fold more GFP^+ neurons in the caudate nucleus, 7-fold in the putamen, and even 50-fold in the midbrain, respectively, compared with the control contralateral side (Fig. 4, K to M).

When the whole putamen was targeted in M3 and M5, numerous GFP^+ neurons were evident throughout the entire anteroposterior and dorsoventral axes, although the pattern of GFP expression was rather focal as compared to the observed Gd enhancement in the same animals (Fig. 5). Delivery of the modified AAV9-hSyn-

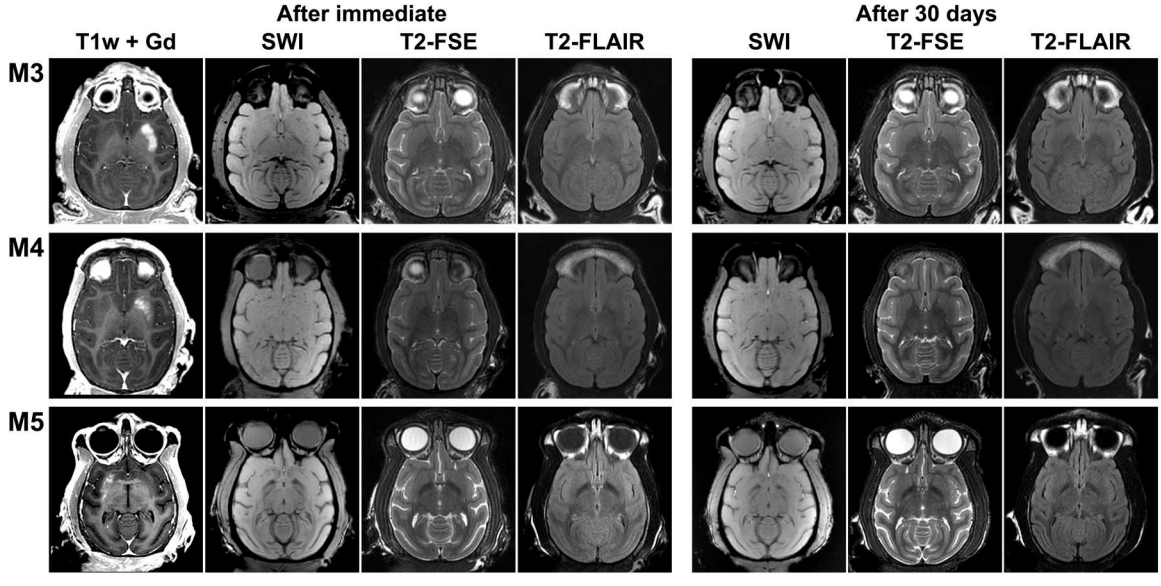

Fig. 3. After immediate and after 30-day safety assessment of large-volume BBB openings in the putamen of normal and parkinsonian NHPs. Follow-up MRI including susceptibility-weighted (SWI), T2*-weighted (T2-FSE), and FLAIR (T2-FLAIR) images in M3, M4, and parkinsonian monkey M5. All images are shown in axial orientation in a single slice corresponding to the largest BBB disruption area, as demonstrated by Gd extravasation. Follow-up sessions were performed immediately and 30 days after treatment.

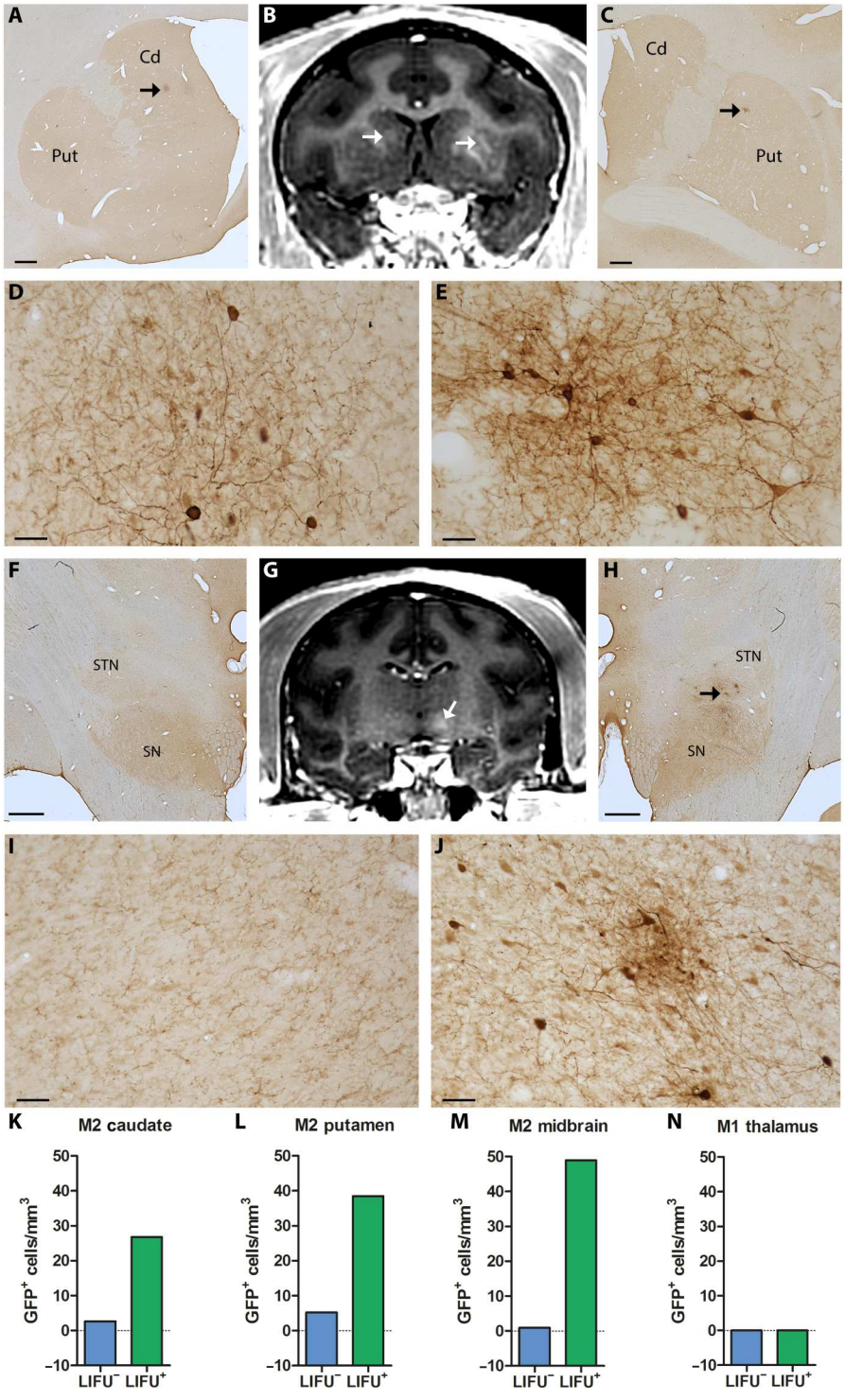

Fig. 4. Multitargeted focal delivery of modified AAV9 vector in the striatum and midbrain. In M2, the distribution areas of GFP^+ cells in the caudate nucleus [**A**, low magnification; **D**, higher magnification taken from the site specified by the arrow in (A)] and the putamen [**C**, low magnification; **E**, higher magnification taken from the site specified by the arrow in (C)] overlap the regions of Gd extravasation observed immediately after sonication (arrows in **B**). Similarly, GFP^+ cells in the midbrain [**H**, low magnification; **J**, higher magnification taken from the site specified by the arrows in (H)] are distributed within the hyperintense BBB-opened area [arrow in (G)]. The same region on the contralateral side served as a negative control showing no hyperintense signal (**G**) or GFP expression (**F** and **I**, low and higher magnification, respectively). Number of GFP^+ cells in the BBB-opened regions ($LIFU^+$) and their contralateral non-opened regions ($LIFU^-$) in the caudate nucleus (**K**), putamen (**L**), and midbrain (**M**) of M2 and in the thalamus of M1 (with NAbs) (**N**). Cd, caudate nucleus; Put, putamen; SN, substantia nigra; STN, subthalamic nucleus. Scale bars, 1 mm (A, C, F, and H) and 50 μm (D, E, I, and J).

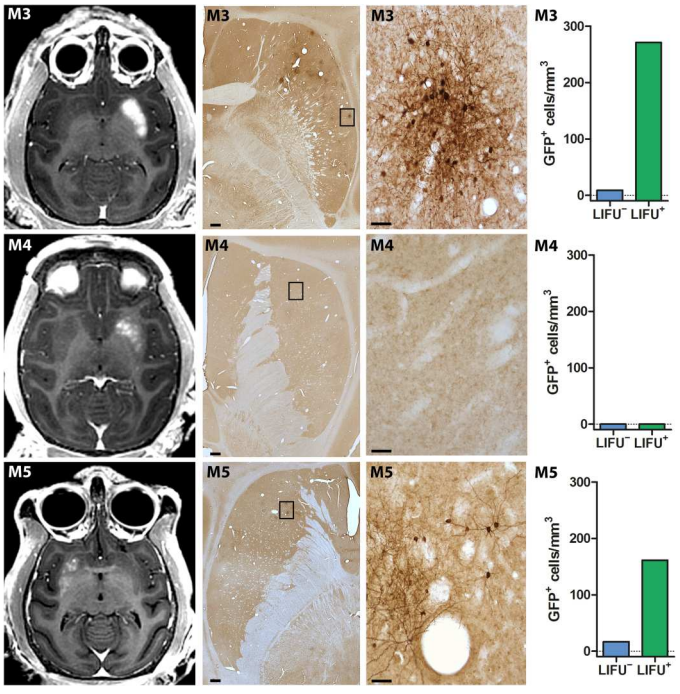

Fig. 5. Delivery of modified AAV9 vectors after large-volume BBB openings in the putamen of normal and parkinsonian NHPs. Representative images of distributions of Gd extravasation (**first column**) and GFP$^+$ cells (low and higher magnifications in **second** and **third columns,** respectively) in the putamen of M3, M4, and parkinsonian monkey M5. Note that the distribution areas of GFP$^+$ cells overlap the regions of Gd extravasation observed immediately after sonication, except for monkey M4 which had NAbs against AAV and, therefore, displayed no GFP expression. **Fourth column** shows the number of GFP$^+$ cells in the BBB-opened regions (LIFU$^+$) and their contralateral non-opened regions (LIFU$^-$) for each monkey. Scale bars, 1 mm (for low magnifications in second column) and 50 μm (for higher magnifications in third column).

GFP vectors resulted in appearance of up to 30- and 10-fold more GFP$^+$ neurons than on the control contralateral side in the normal (M3) and parkinsonian (M5) monkeys, respectively (Fig. 5). Overall, the number of GFP$^+$ neurons was likely associated with the extent of BBB openings as quantified with Gd T1-weighted images in all the monkeys, including M2; the larger the opening, the greater the number of GFP$^+$ neurons (Figs. 4 and 5). Thus, the data indicate that multitargeted focal AAV vector delivery and resultant protein expression in association with BBB opening volumes are safe and feasible in adult NHPs.

The GFP$^+$ neurons were immunostained for neuronal nuclei (NeuN, neuronal marker), glial fibrillary acidic protein (GFAP; astroglial marker), and ionized calcium binding adapter molecule 1 (Iba1; microglial marker) to ascertain the neuron specificity of GFP expression induced by the AAV9-hSyn-GFP vectors. Neurons clearly displayed GFP expression, whereas neither astroglia nor microglia exhibited GFP expression (Fig. 6), thus demonstrating the neuron-specific expression under hSyn promotor control.

Tissue assessment following LIFU BBB openings and AAV vector delivery

Both hemispheres (treated and untreated) appeared intact visually on macroscopic examination. Nissl staining revealed no microscopic hemorrhage, necrosis, or abnormal cell morphology (Fig. 7). Our Nissl-stained cell counts in all targeted regions of all monkeys were equivalent to those in their corresponding non-opened regions on the contralateral side (Fig. 7 and fig. S5). Overall, there were no substantial changes in microglial or astroglial markers, nor any other histological abnormalities in four (M1, M2, M4, and M5) of the five monkeys, as compared to the untreated contralateral side. In these animals, GFAP staining showed the absence of broad gliosis, and Iba1-positive cells qualitatively appeared to have normal morphology within the targeted areas (Fig. 7). A minor increase in GFAP-positive cells around peripheral blood vessels was observed in the putamen of M4. In M3, on the other hand, there were moderate increases in both GFAP- and Iba1-positive cells, especially in the anterior putamen (Fig. 7). This region was the same that had shown a sparse distribution of Gd uptake by MRI 30 days after the large-volume BBB opening (Fig. 2A). However, the findings were limited to small zones, and neurons in the surrounding tissues of the putamen seemed intact.

In vivo PET imaging of BBB permeability using ^{18}F-Choline in NHPs and patients with PD

Delivery of the modified AAV9-hSyn-GFP vectors into the putamen led to net neuronal protein expression. However, we observed some divergence between the large area covered with Gd (nearly the whole putamen) and the smaller limited regions where GFP expression was evident. We therefore attempted an additional approach to test the possible functional value of BBB opening. To this end, we used PET imaging with ^{18}F-Choline, a radiotracer unable to cross the BBB in normal physiological conditions. It is well known that PET is a sensitive and quantitative molecular imaging technique that can measure probe distribution and uptake and pharmacokinetics of drug delivery within the brain (*37*).

Large-volume LIFU BBB openings were performed unilaterally in the putamen and midbrain simultaneously in one additional monkey (M6), and then ^{18}F-Choline PET imaging was carried out to demonstrate the effective intraparenchymal delivery and active biodistribution of the probe. The targeted BBB openings were successful for both the putamen (730 mm^3) and the midbrain (215 mm^3). We found that ^{18}F-Choline entered only the regions that were markedly permeabilized by the BBB openings (Fig. 8A). Consistently, LIFU induced a 90% increase in ^{18}F-Choline uptake in the putamen and a 61% increase in the midbrain, as compared to their corresponding non-opened regions on the contralateral side (see table S2).

Analogously, BBB openings in the postcommissural putamen and/or midbrain were also performed in patients with PD as part of broader clinical trials (ClinicalTrials.gov, no. NCT03608553; see table S3). The same ^{18}F-Choline PET imaging was carried out separately in three patients after BBB opening of the unilateral putamen, the bilateral putamen, or the unilateral putamen and midbrain region, respectively (see Material and Methods and tables S4 and S5 for methodological details and procedure-related parameters). In these patients, the increase in ^{18}F-Choline uptake was also quite noticeable (up to 60 and 39% uptake increase in the putamen and midbrain, respectively) in keeping with the degree of BBB opening revealed by Gd enhancement (Fig. 8B, fig. S6, and table S2). Because ^{18}F-Choline uptake requires the radiotracer to bind to cell membrane, our findings indicate its effective penetrance into the targeted brain regions.

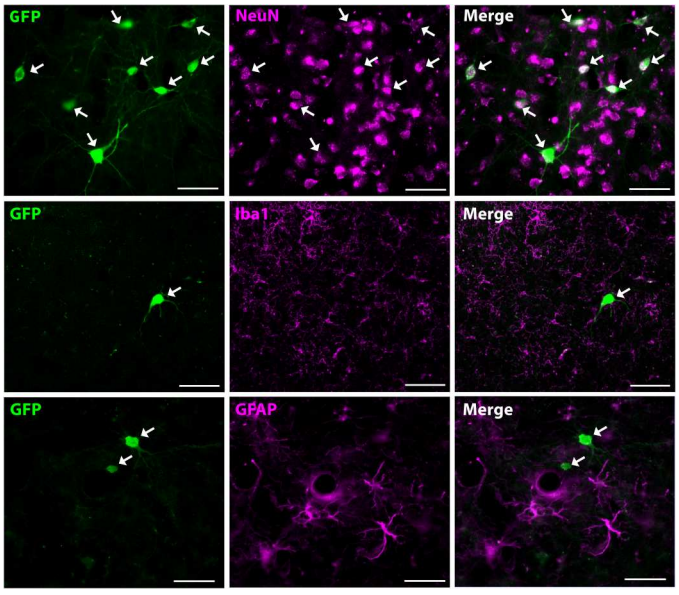

Fig. 6. Neuron specificity of AAV vector–induced transgene expression. Colocalization with the neuronal marker NeuN (**top row**), but not with the microglial marker Iba1 (**middle row**) or astroglial marker GFAP (**bottom row**) in GFP$^+$ cells indicates that GFP is expressed specifically in neuronal cells. Scale bars, 50 μm.

DISCUSSION

We report that BBB opening with LIFU in brain regions relevant to PD in NHPs and human patients is safe and can be performed precisely in accordance with predesigned targets, including bilateral approaches. Our study shows that systemically administered AAV vectors can be delivered successfuly into focal targeted regions of adult NHPs, leading to neuronal protein expression and thus giving rise to potential therapeutic target engagement. In contrast to the rodent brain, enhanced transgene expression in NHP brain after systemic vector administration has been challenging (*24*–*27*).

Both animals and patients tolerated the procedure perfectly well, and we found no evidence for neurological, behavioral, or general complications. Postmortem assessment of the monkey brain revealed that the BBB opening procedure did not cause apparent tissue damage. Exceptionally, in one animal with the largest opening in the putamen, we encountered some inflammatory changes 1 month later. However, the observed inflammatory response was limited minimally to a specific focal region (i.e., anterior putamen) where the BBB opening was initially more intense and longer lasting. Inflammation secondary to BBB opening has been described as reversible and relatively short-lasting (*38*, *39*). Several studies suggest that permanent tissue damage is avoidable when the appropriate ultrasound setting and microbubble dose are used (*40*). It is noteworthy that our BBB opening was safe and seemed unassociated with any tissue damage in the striatum of a PD monkey model.

Our experience with NHPs raises some considerable issues regarding gene transfer and protein expression. The first is the characteristics of viral vectors. Here, two types of modified AAV9 vectors, AAV9-PHPeB and AAV9.2-PHPeB vectors, were used, and both vectors under hSyn promotor control were found to work similarly and successfully to induce neuronal protein expression. This might be ascribable to the excellent gene transfer

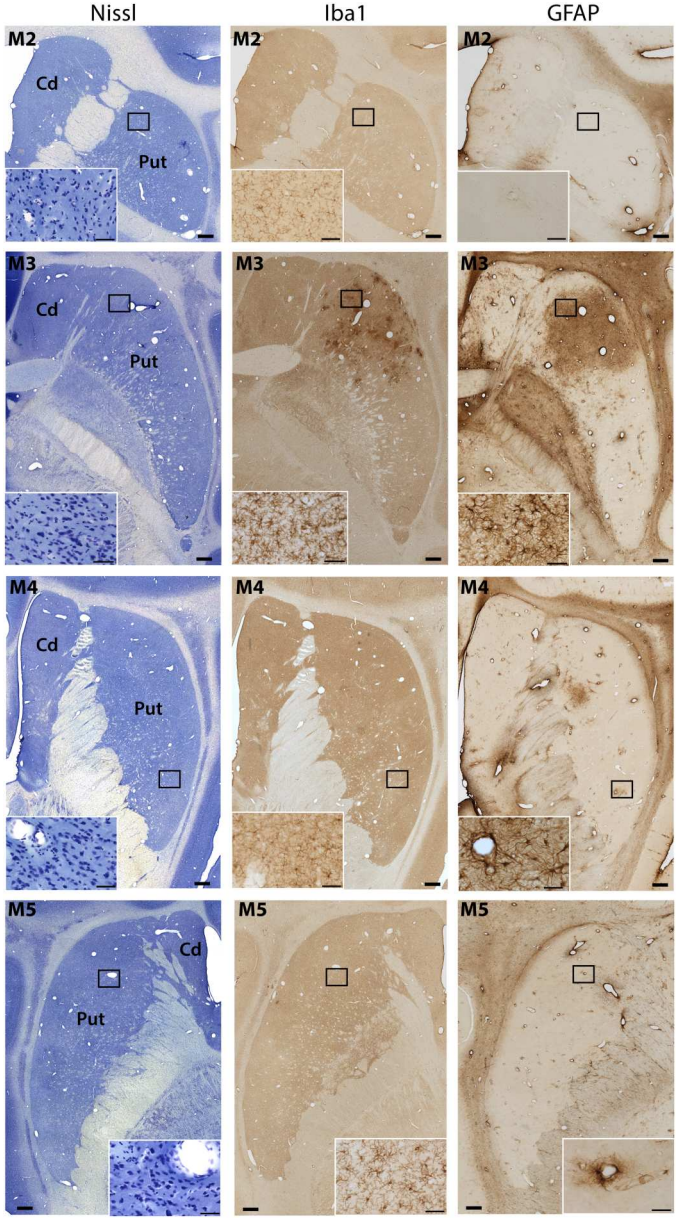

Fig. 7. Tissue assessment following LIFU BBB openings and AAV vector delivery. Three adjacent sections were processed for Nissl staining **(left column)** and immunostaining for Iba1 **(central column)** and GFAP **(right column)** following LIFU BBB openings and AAV vector delivery in M2, M3, M4, and parkinsonian M5. No marked histopathological changes were observed, except for M3 who exhibited minor focal inflammation but no tissue distortion in the BBB-opened area. Scale bars, 1 mm and 50 μm (insets).

efficiency of the modified vectors (vectors based on AAV9 variants) via their systemic administration. The second is the importance of NAbs against AAV (*41*). The presence of these circulating NAbs affects protein expression in the brain (*35*, *36*). This is quite critical practically, since around 50% of the human population is known to have NAbs against AAV in serum (*42*). The third is the extent of neuronal protein expression. We have found that GFP expression following large-volume BBB opening was up to 30 to 50 times greater in the opened putamen and midbrain than in the non-

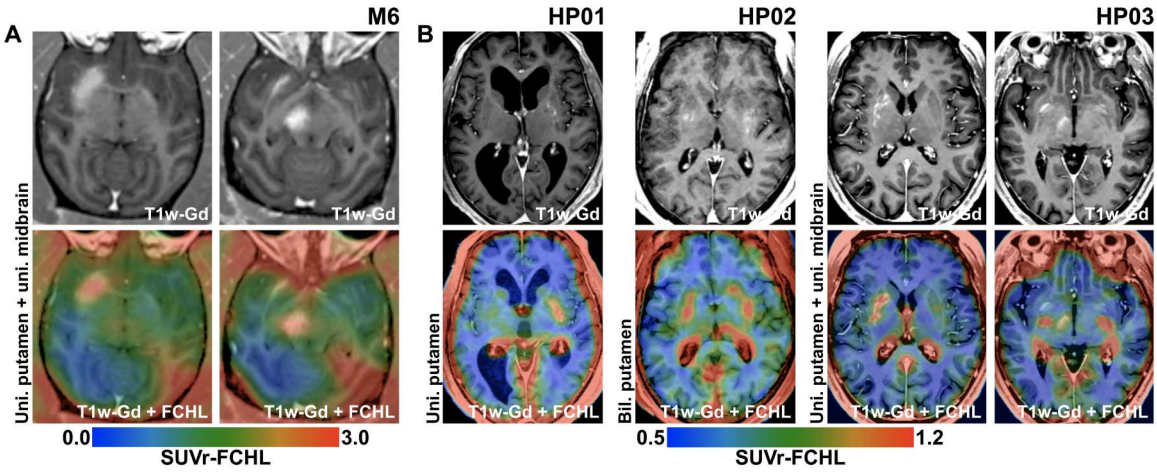

Fig. 8. In vivo PET imaging of BBB permeability using ^{18}F-Choline in NHPs and patients with PD. Data obtained in monkey M6 (**A**) and three patients with PD (**B**) are included. The top row shows targeted regions on T1-weighted images with Gd extravasation after BBB opening sessions. The bottom row depicts colored overlays of ^{18}F-Choline PET images and the T1-weighted images. PET images are represented in blue-green-red colormaps, where red indicates the highest uptake value. Increased ^{18}F-Choline uptake is seen only in the regions where net BBB opening occurred, such as the putamen and midbrain in M6 (A) and unilateral putamen (HP01), bilateral putamen (HP02), and the unilateral putamen and midbrain (HP03) in patients with PD (B).

opened contralateral sites. However, the degree of GFP expression may probably be still too limited [as involving a relatively low proportion of neurons (*43*)] to be considered therapeutically valid. Such somewhat restricted GFP expression despite the large-volume BBB opening (as assessed by both MRI and ^{18}F-Choline PET imaging) is a crucial point to resolve. In this context, it has recently been reported in rodents that the serotypes of AAV vectors, the extent of LIFU-induced BBB permeability, and the intrinsic properties of the targeted brain tissue influence the efficacy of neuronal transduction via the vectors and the biodistribution and diffusion of transduced neurons (*36*, *44*). There are major differences in the degree of vector-induced transgene expression between rodents and primates (*26*, *27*, *36*). Achieving efficient gene transfer in the primate brain is more challenging and might be related to a series of factors. It is noteworthy that therapeutic levels of transgene expression could be attained, since the vector dose currently used for gene delivery to human brains is much higher (*45*).

In this study, we also show that ^{18}F-Choline PET imaging provides a valid approach to assess BBB opening at the molecular level in both NHPs and patients with PD. ^{18}F-Choline uptake is mediated by binding to cell membrane (*46*, *47*). Therefore, robust uptake seen only after BBB opening in the putamen, and midbrain is indicative of entry into the brain parenchyma, including bilateral/simultaneous putamen and midbrain uptake. Admittedly, exactly to which cell components ^{18}F-Choline binds is still unknown and requires further investigation. Equally, the effects of LIFU BBB opening on cell receptors, transport mechanisms, and vascular systems remain uncertain. Nevertheless, PET imaging may be a useful tool to explore possible mechanisms underlying BBB opening, such as metabolic activity, uptake, distribution, and pharmacokinetics of drug delivery into the brain (*48*, *49*). Moreover, BBB opening together with PET imaging could be potentially applied to assess cellular markers of neurodegeneration in future studies.

Our experience indicates that a minimally invasive methodology can be effectively put forward to conceive molecular therapies for neurodegenerative disorders. We have concentrated on the putamen and midbrain (i.e., SNc), because nigrostriatal dopaminergic degeneration is the most important pathogenic feature of PD early in its evolution (*31*). Opening these principal areas is feasible, reproducible, safe, and functionally successful in both NHPs and patients with PD. Of note, we used the same focused ultrasound equipment.

One of the advantages of gene therapy is that AAV vector delivery would probably be needed only once over a long time period, which is a major benefit as compared to other emerging drug therapies that might require more frequent (i.e., monthly) treatments. It is worth considering that gene therapy (or other potential therapeutic approaches) for PD does not necessarily have to be restricted to the nigrostriatal system. For instance, the enzyme glutamic acid decarboxylase that leads to GABA synthesis and, therefore, to neuronal inhibition, has been delivered by direct injection into the subthalamic nucleus in PD patients with some degree of success (*50*). This approach requires surgical intervention bilaterally, which is probably too invasive to be considered in the early stages of the disease. Our data reveal that the subthalamic nucleus and other pathophysiologically relevant sites, including the motor cortical and thalamic areas, could also be targeted for drug delivery. One might conceive a double-hit approach early in PD, whereby BBB opening could be used to recover from functional abnormalities in the cortico-basal ganglia motor circuit, while a neuroprotective therapy could be directed toward the nigrostriatal system (*32*).

In conclusion, this study provides evidence for minimally invasive intracerebral AAV vector focal delivery across the BBB in adult NHPs using LIFU. This has broad implications for the fields of gene therapy and neurodegeneration. Targeted focal BBB opening might be envisaged as a valid approach to various putative neurorestorative therapies that should be tested in a wide range of central nervous system disorders.

MATERIALS AND METHODS

Animals

Six male macaque monkeys (*Macaca fascicularis*), weighing 3 to 10 kg, aged 3 to 8 years, and sourced from Hartelust BV (Tilburg, The Netherlands), were used in this study. Animals were housed in an animal room under standard conditions and treated in accordance with the European and Spanish guidelines (86/609/EEC and 2003/65/EC European Council Directives and the Spanish Government). The experimental protocol was approved by the Ethical Committee for Research of the Fundacion de Investigacion HM Hospitales (CEEA-02/2019) and of Comunidad de Madrid (PROEX 283/2019). One monkey (M5) was treated with two doses of MPTP (0.5 mg/kg, i.v.) as described before (*51*) but maintained rather normal motor features until sacrifice. Water and fresh fruit were available ad libitum. Qualified health care personnel oversaw the monkeys′ welfare throughout the studies.

MRI acquisition

MRI for planning and evaluation was acquired in a 3T MR system (Discovery 750w; GE Healthcare, Milwaukee, WI). NHPs were placed on the MR table in sphinx position, and MRI protocols were acquired using a flexible 16-channel coil array. The baseline protocol included only a high-resolution T1-weighted fast spoiled gradient-echo (FSPGR) with 0.6 mm of isotropic spatial resolution for target definition. The follow-up protocol included, in addition to the high-resolution FSPGR, T2-FSE, FLAIR, SWI, DWI, and T2*-weighted gradient recalled echo (GRE), and all of which were used to evaluate tissue integrity after sonication for edema (T2-FSE and FLAIR), microhemorrhage (SWI), and infarction (DWI). To assess the efficacy of BBB opening, a paramagnetic Gd-derived contrast agent (Gadovist) was given intravenously (0.2 ml/kg), and additional T1-weighted FSPGR (T1w-Gd) images were acquired 10 min after administration. Follow-up MRI was generally acquired immediately after the BBB opening procedure in all NHPs, and either at 24 hours or 30 days postsonication. During MRI scanning, the animals were anesthetized with a mixture of ketamine (10 mg/kg) and midazolam (1 mg/kg) and maintained during the 10-min-long scanning period with half of the initial dose per hour.

LIFU procedure

In preparation for the LIFU procedure using the clinical setup, the animal was anesthetized, the head was shaved, and an intravenous catheter was placed in the saphenous vein. Initial anesthesia was done with a mixture of ketamine (10 mg/kg) and midazolam (1 mg/kg) and maintained during the LIFU procedure with half of the initial dose per hour. The animal was covered with a blanket and insulating material to preserve body temperature during the whole procedure.

BBB opening was performed with an MR-guided focused ultrasound device (ExAblate Neuro; InSightec, Haifa, Israel) with a 1024-element phased-array transducer (220-kHz fundamental frequency). The transducer was tilted in horizontal position (pointing upward) to facilitate animal positioning. Before positioning the animal, the transducer was filled with degassed cold water. The whole procedure lasted approximately 90 to 120 min and involved intraprocedure MRI acquisition, target definition, microbubble delivery, and low-intensity pulsed sonications.

Intraprocedure MRI, a three-dimensional fast GRE BRAVO, was acquired and realigned to baseline MRI previously determined for target definition. Several targets were attempted at different anatomical locations (see table S1). Targets were defined directly on the baseline T1-weighted high-resolution MRI as a grid of spots with predefined spacing of 1 to 2 mm. Microbubbles (Luminity, 4 μl/kg/ml in physiological saline) were infused through a catheter using an MRI-compatible infusion pump at a rate of 0.02 ml/s. Infusion was started 3 to 4 min before application of the first low-intensity pulsed sonication. Acoustic power was fixed to 1 W, without using a system controller for a predefined microbubble activity dose according to a previous study that showed a good compromise between BBB opening success and safety (*22*). Sonications were delivered during 60 to 150 s per target grid (table S1). Cavitation activity in the subharmonic frequency band was monitored and quantified along with the sonication, as previously reported (*8*, *13*). At the end of each sonication, single-slice T2*-weighted MRI centered on the target location was acquired and visually inspected to control for the presence of any possible abnormality and T2* hypointensities. Once the procedure was completed and all targets were sonicated, monkeys were taken off the ExAblate and transferred to the MR bed for MRI acquisition of the follow-up protocol. Two monkeys (M1/M5) received a single dose of methylprednisolone (10 mg/kg, i.m.) after completing MR sequence acquisition.

Initially, two monkeys (M1/M2) were used for optimization of the BBB opening versus safety trade-off, particularly regarding treatment parameters (sonication power and duration, microbubble concentration, and activity target dose) and T2* hypointensities (*31*). This experience allowed us to better define the approach of BBB opening and specifically led to a conservative method to avoid any hint of tissue damage as previously suggested (*22*).

Viral production, injection, and analysis of basal levels of endogenous antibodies

Two types of modified AAV9 vectors, AAV9-PHPeB and AAV9.2-PHPeB vectors (*52*), were produced by the helper-free triple transfection process. Briefly, AAV-293 cells (70% confluent in Corning Cell Stack 10 chamber) were transfected by genome helper (pHelper; Stratagene, San Diego, CA) and packaging plasmids (pAAV-RC9-PHPeB and pAAV-RC2) with polyethylenimine (PEI Max; Polysciences, Warrington, PA). For production of the AAV9.2-PHPeB vector, the pAAV-RC9-PHPeB plasmid-coding AAV9-PHPeB capsid protein and the pAAV-RC2 plasmid-coding AAV2 capsid protein were transfected in a ratio of 9:1, respectively (*53*). The produced vectors were then purified by CsCl gradient. Viral titers were determined by quantitative polymerase chain reaction using Taq-Man technology (Life Technologies, Gaithersburg, MD). The purity of the vectors was assessed by 4 to 12% SDS–acrylamide gel electrophoresis and fluorescent staining (Oriole; Bio-Rad, Hercules, CA). The transfer plasmid (pAAV-hSyn-AcGFP-WPRE) was constructed by inserting the hSyn promotor sequence and *AcGFP* gene with the WPRE sequence into an AAV backbone plasmid (pAAV-MCS; Stratagene, La Jolla, CA).

Within 2 hours after sonication, a vector solution (5.0×10^{13} vg) was infused slowly through the saphenous vein in the monkeys under anesthesia. This time frame corresponds to the posttreatment MRI acquisition protocol to confirm successful BBB opening and discard abnormalities, such as edema, microhemorrhage, and infarction. The amount of AAV vectors injected was determined on

the basis of previous reports on their intravenous infusions in macaque monkeys (*27*, *36*, *54*). After the infusion, the monkeys were monitored until full recovery from anesthesia.

Detection of AAV9 NAbs was assessed in primate serum before vector injection, as previously described (*55*, *56*). Briefly, two V6.11 cells (American Type Culture Collection, Manassas, VA) were seeded onto 96-well cell culture plates at a density of 3×10^4 cells per well and induced with ponasterone A (Life Technologies) at a concentration of 1 mg/ml. The next day, heat-inactivated serum was diluted (1:2, 1:4, 1:8, and 1:16) in heat-inactivated fetal bovine serum and mixed directly with an equal amount of Dulbecco's modified Eagle's medium–diluted AAV-CMV-AcGFP vector (1.0×10^{10} genome copy per well) in triplicate. The serum-vector mixtures were incubated at 37°C for 1 hour. The mixtures were then added to cells and allowed to incubate overnight. The fluorescent intensity of each well was measured on a Cytation 5 plate reader (Agilent, Santa Clara, CA), and percent inhibition was calculated with a no-antibody control sample as a reference. The titer of AAV9 NAbs was determined as the highest serum dilution showing over 50% inhibition.

Postmortem procedures

Five monkeys (M1 to M5) were anaesthetized deeply with sodium pentobarbital (10 mg/kg, i.p.) and perfused transcardially through the ascending aorta with physiological saline, followed by 4% paraformaldehyde dissolved in phosphate buffer and a series of phosphate-buffered sucrose solutions (5 to 10 to 20%) and then cryoprotected in 30% phosphate-buffered sucrose (*51*). Brains were blocked in the coronal (M1/M2) or axial (M3/M4/M5) plane and sectioned on a freezing microtome at 40 μm to produce 10 adjacent series.

Free-floating 40-μm-thick coronal or axial sections were washed in tris buffer and treated with citrate buffer (pH 6) for 30 min at 37°C for antigen retrieval. Inhibition of endogenous peroxidase activity was performed using a mixture of 10% methanol and 3% concentrated H_2O_2 for 20 min. Normal serum was applied for 3 hours for blocking nonspecific binding sites.

The sections were incubated at 4°C for a duration of 72 hours with primary antibodies directed against tyrosine hydroxylase (TH; mouse MAB5280 Millipore, RRID:AB_220152; 1:1000), GFP (rabbit A6455 Thermo Fisher Scientific, RRID:AB_221570; rabbit G10362 Thermo Fisher Scientific, RRID:AB_2536526; 1:1000), Iba1 (rabbit 019-19741 Wako, RRID:AB_839504; 1:1000), and GFAP (mouse Ab4648 Abcam, RRID:AB_449329; 1:2000).

The sections were washed in tris-buffered saline and transferred for 2 hours to a solution containing the corresponding secondary biotinylated antibody (goat anti-rabbit AP232B Chemicon, RRID:AB_11212148; 1:400; or horse anti-mouse BA2000 Vector Laboratories, RRID:AB_2313581; 1:400). Afterward, they were incubated for 45 min with the avidin-biotin-peroxidase complex (ABC Vectastain; Vector Laboratories). Immunohistochemical reaction products were visualized by incubating the sections with 0.05% 3,3′-diaminobenzidine (Sigma-Aldrich) and 0.003% H_20_2. The sections were then dehydrated through graded ethanols and defatted in two changes of xylene before being coverslipped with DePeX (Serva) as a mounting medium. Omission of the primary antibodies resulted in non-immunostaining (images not shown).

To assess the neuron specificity of AAV vector–induced transgene expression, double immunofluorescence of GFP were performed either with the neuronal marker NeuN (mouse MAB377 Millipore, RRID:AB_2298772; 1:500), Iba1, or GFAP. Sections were blocked with normal serum for 3 hours before being incubated 72 hours with primary antibodies. Secondary fluorescent antibodies (Alexa Fluor goat anti-rabbit 488, RRID:AB_143165; 1:500; Alexa Fluor goat anti-mouse 568, RRID:AB_2534072; 1:500; Alexa Fluor goat anti-rabbit 568, RRID:AB_143157; 1:500; Invitrogen) were used. The sections were then dehydrated through graded ethanols and defatted in two changes of xylene before being coverslipped with DPX as a mounting medium. Epifluorescence images of GFP and subsequently NeuN, Iba1, or GFAP were acquired on a Leica DM 2500 microscope (Leica, Germany) at ×40 magnification. Images were acquired at different focal depths and then merged into an overlay image using the Leica Application Suite X software.

Analysis of neuron density in Nissl-stained sections

The sections were processed as previously described and incubated in 70% ethanol overnight. After a quick wash in distilled water, they were incubated at 45°C in agitation with 0.1% cresyl violet for 5 min. Following another quick wash in distilled water, the sections were incubated in sequential solutions of 70% ethanol for 1 min, 96% ethanol for 1 min, and chloroform for 10 min (in agitation) and then washed in 96% ethanol. Last, the sections were incubated in the differentiation solution under visual control and rapidly washed in 100% ethanol before being incubated in clean xylol 6 × 10 min and coverslipped with DPX.

Neuron density in the putamen was quantified using the Auto Local Threshold and Analyze Particles functions of ImageJ 1.53a software (National Institutes of Health, USA). Images were acquired on the Leica DM 2500 microscope at ×10 magnification. At least 40 random fields taken from five to six sections for each hemisphere were quantified. Neuronal cells were filtered from glial cells by using the "default" method and "50-infinity" size filters. Data were expressed as a percentage of the total Nissl-stained area and normalized to the control contralateral hemisphere.

Stereological analysis

In M1 and M2, the number of GFP^+ neurons on coronal sections (see Fig. 4) was assessed by stereology with the optical fractionator method in a total of 15 sections regularly spaced at intervals of 800 μm through the caudate nucleus and putamen, 8 sections through the thalamus, and 10 sections of the midbrain regularly spaced at intervals of 400 μm. The midbrain included sections from the more anterior part of the STN to the more posterior region of the SNc. In M3, M4, and M5, the number of GFP^+ neurons on axial sections (see Fig. 5) was assessed in a total of 12 sections regularly spaced at intervals of 800 μm, covering the entire rostrocaudal and dorsoventral axes of the putamen. Stereological estimations were carried out by using a computer-assisted image analysis system consisting of a microscope (Olympus BX3) equipped with a computer controlled motorized stage, a camera, and StereoInvestigator software (Stereo Investigator 2017; MicroBrightField, Williston, VT, USA). All regions were outlined at ×2 magnification, and immunolabeled cells were counted with ×40 magnification (counting frame, 200 μm by 200 μm; sampling grid, 1000 μm by 1000 μm for the putamen and 400 μm by 400 μm for the caudate nucleus and midbrain). After counting was finished, the total number of neurons

was automatically calculated by the software using the formula described by West (*57*).

Assessment of TH-positive fiber density in the putamen

The relative optical density of TH-positive fibers in the putamen was quantified using computer-assisted image analysis techniques (ImageJ 1.53a; National Institutes of Health, USA) as previously described (*51*). Briefly, images were captured with an Olympus BX3 microscope and converted to black and white 8-bit monochrome. Digital images were captured under the same exposure settings for all experimental cases. Seven axial consecutive sections covering the whole dorso-ventral axis, regularly spaced at intervals of 1600 μm, were examined for each monkey. The optical density of a non-stained region in the same section was subtracted as background. The percent reduction of TH-positive fiber density was determined as percent loss in the MPTP-treated monkey compared with the value for one control monkey in the same region.

Patients and procedures

The study was approved by the Research Ethics Board at HM Hospitales (20.12.1101E6-GHM) and the Spanish Agency of Medicines and Medical Products (627/17/EC). The study design and conduct complied with all relevant regulations regarding the use of human study participants and conformed to the principles of the Declaration of Helsinki. All patients and their legal representatives provided written informed consent to participate in the study.

Three patients (age range: 63 to 78; years since diagnosis: 5 to 8) with PD and cognitive impairment were studied (clinical details in table S3) and underwent LIFU BBB opening as part of a prospective single-arm, nonrandomized, proof-of-concept phase 1 clinical trial (ClinicalTrials.gov, no. NCT03608553) designed to investigate the safety and feasibility of focal BBB opening in patients with PD. Details of the procedure have been previously reported (*13*, *14*). Relevant to this study, the microbubble contrast agent (Luminity) was administered by gravitational infusion instead of intravenous bolus injection. Microbubbles were activated, and a volume of 1.3 to 1.5 ml was diluted in 50 ml of saline. An infusion rate of 2.5 ml/min was manually controlled using an infusion rate monitor (DripAssist, Shift Labs). Further infusion parameters are detailed in table S4. Targets for LIFU sonications were defined on intraprocedural acquisitions using an interspot spacing of 2 to 3 mm. Targets varied among the subjects as follows: the unilateral postcommissural putamen (HP01), the bilateral postcommissural putamen (HP02), and a multitarget approach including the unilateral putamen and substantia nigra (HP03). Putaminal boundaries were identified on T1-weighted axial and coronal MRI, while the substantia nigra could be observed on axial SWI. LIFU sonications were started 3 to 4 min after the start of microbubble administration to allow for steady-state concentration in blood. Maximum power was set at 15 W, and sonication duration varied between 100 and 180 s. Cavitation activity was monitored and quantified along with the sonication as described elsewhere (*14*). Because of the lack of human data on microbubble infusion, we defined a conservative lower target for cavitation accumulated dose (0.5 to 0.7) as compared to our previous reports (*13*, *14*) (see also table S5 for further details regarding target definition, sonication parameters, and cavitation dose outcomes). As in NHPs, during each sonication, single-slice T2*-weighted MRI was acquired and visually inspected to control for T2* hypointensities. Again, in the case of any detected or suspicious hypointensities, even when the predefined cavitation dose was not achieved, no further ultrasound was delivered to the same target. Once the procedure was completed (the objective cavitation dose reached all targets), the patients were transferred to the MR bed, and a brain MRI protocol including the same sequences as used in the NHP experiments was acquired. The patients were clinically monitored afterward before going to the ward. They were mildly sedated, and medical surveillance was maintained during the procedure by a specialized physician.

^{18}F-Choline PET imaging studies

One monkey (M6) and all three human PD patients underwent ^{18}F-Choline PET imaging once BBB opening was confirmed on T1w-Gd images. Subjects were transferred to a hybrid PET-MRI scanner (mMR Biograph; Siemens, Erlangen) for PET acquisition, which started immediately following the intravenous injection of FCH radiotracer (~2 mCi in the monkey and ~5 mCi in humans). On average, ^{18}F-Choline PET acquisition was started around 1 hour after finalizing the BBB procedure. Forty minutes of PET was acquired in list mode. PET emission data were reconstructed with an ordered subset-expectation maximization algorithm and corrected for attenuation using subject-specific multicompartment MR-based maps (*58*). PET activity between 10 and 40 min was reconstructed in a single frame and converted to standardized uptake value ratios (SUVr) taking a cerebellar mask as a reference region. Subsequently, several spherical regions of interest (ROIs) were drawn on a high-resolution T1w-Gd MRI showing enhanced contrast in the areas where the BBB was opened. For patients, ROIs were placed on the posterior putamen (radius, 5 mm), anterior caudate nucleus (radius, 5 mm), and substantia nigra (radius, 4 mm) bilaterally. For the monkey (M6), the defined ROIs were placed on the posterior putamen (radius 4 mm) and substantia nigra (radius 3 mm). SUVr were averaged in all ROIs, and ^{18}F-Choline SUVr were normalized to contralateral (control) regions. In the case of bilateral targeting (HP02), ^{18}F-Choline SUVr were normalized to the ipsilateral caudate region.

Statistical analysis

Results are reported as an average per hemisphere (mean ± SEM). All statistical analyses were performed using the GraphPad Prism software. For Nissl-stained sections, a two-tailed unpaired Student *t* test was performed to determine differences between each of the hemispheres. For TH analysis, a two-tailed unpaired Student *t* test was performed to determine differences between the control and the MPTP-treated monkey. In both cases, two-sided *P* values of less than 0.05 were considered significant.

Supplementary Materials

This PDF file includes:

Figs. S1 to S6
Tables S1 to S5

View/request a protocol for this paper from *Bio-protocol*.

REFERENCES AND NOTES

1. G. Deuschl, E. Beghi, F. Fazekas, T. Varga, K. A. Christoforidi, E. Sipido, C. L. Bassetti, T. Vos, V. L. Feigin, The burden of neurological diseases in Europe: An analysis for the Global Burden of Disease Study 2017. *Lancet Public Health* **5**, e551–e567 (2020).

2. R. Daneman, A. Prat, The blood–brain barrier. *Cold Spring Harb. Perspect. Biol.* **7**, a020412 (2015).
3. A. Akhtar, A. Andleeb, T. S. Waris, M. Bazzar, A.-R. Moradi, N. R. Awan, M. Yar, Neurodegenerative diseases and effective drug delivery: A review of challenges and novel therapeutics. *J. Control. Release* **330**, 1152–1167 (2021).
4. V. Sudhakar, R. M. Richardson, Gene therapy for neurodegenerative diseases. *Neurotherapeutics* **16**, 166–175 (2019).
5. C. N. Bedbrook, B. E. Deverman, V. Gradinaru, Viral strategies for targeting the central and peripheral nervous systems. *Annu. Rev. Neurosci.* **41**, 323–348 (2018).
6. M. Hocquemiller, L. Giersch, M. Audrain, S. Parker, N. Cartier, Adeno-associated virus-based gene therapy for CNS diseases. *Hum. Gene Ther.* **27**, 478–496 (2016).
7. R. C. Challis, S. Ravindra Kumar, X. Chen, D. Goertsen, G. M. Coughlin, A. M. Hori, M. R. Chuapoco, T. S. Otis, T. F. Miles, V. Gradinaru, Adeno-associated virus toolkit to target diverse brain cells. *Annu. Rev. Neurosci.* **45**, 447–469 (2022).
8. N. Lipsman, Y. Meng, A. J. Bethune, Y. Huang, B. Lam, M. Masellis, N. Herrmann, C. Heyn, I. Aubert, A. Boutet, G. S. Smith, K. Hynynen, S. E. Black, Blood-brain barrier opening in Alzheimer's disease using MR-guided focused ultrasound. *Nat. Commun.* **9**, 2336 (2018).
9. A. R. Rezai, M. Ranjan, P.-F. D'Haese, M. W. Haut, J. Carpenter, U. Najib, R. I. Mehta, J. L. Chazen, Z. Zibly, J. R. Yates, S. L. Hodder, M. Kaplitt, Noninvasive hippocampal blood-brain barrier opening in Alzheimer's disease with focused ultrasound. *Proc. Natl. Acad. Sci. U.S.A.* **117**, 9180–9182 (2020).
10. P.-F. D'Haese, M. Ranjan, A. Song, M. W. Haut, J. Carpenter, G. Dieb, U. Najib, P. Wang, R. I. Mehta, J. L. Chazen, S. Hodder, D. Claassen, M. Kaplitt, A. R. Rezai, β-amyloid plaque reduction in the hippocampus after focused ultrasound-induced blood-brain barrier opening in Alzheimer's disease. *Front. Hum. Neurosci.* **14**, 593672 (2020).
11. S. H. Park, K. Baik, S. Jeon, W. S. Chang, B. S. Ye, J. W. Chang, Extensive frontal focused ultrasound mediated blood-brain barrier opening for the treatment of Alzheimer's disease: A proof-of-concept study. *Transl. Neurodegener.* **10**, 44 (2021).
12. A. Abrahao, Y. Meng, M. Llinas, Y. Huang, C. Hamani, T. Mainprize, I. Aubert, C. Heyn, S. E. Black, K. Hynynen, N. Lipsman, L. Zinman, First-in-human trial of blood–brain barrier opening in amyotrophic lateral sclerosis using MR-guided focused ultrasound. *Nat. Commun.* **10**, 4373 (2019).
13. C. Gasca-Salas, B. Fernández-Rodríguez, J. A. Pineda-Pardo, R. Rodríguez-Rojas, I. Obeso, F. Hernández-Fernández, M. Del Álamo, D. Mata, P. Guida, C. Ordás-Bandera, J. I. Montero-Roblas, R. Martínez-Fernández, G. Foffani, I. Rachmilevitch, J. A. Obeso, Blood-brain barrier opening with focused ultrasound in Parkinson's disease dementia. *Nat. Commun.* **12**, 779 (2021).
14. J. A. Pineda-Pardo, C. Gasca-Salas, B. Fernández-Rodríguez, R. Rodríguez-Rojas, M. del Álamo, I. Obeso, F. Hernández-Fernández, C. Trompeta, R. Martínez-Fernández, M. Matarazzo, D. Mata-Marín, P. Guida, A. Duque, D. Albillo, I. P. d. I. Heras, J. I. Montero, G. Foffani, G. Toltsis, I. Rachmilevitch, J. Blesa, J. A. Obeso, Striatal blood–brain barrier opening in parkinson's disease dementia: A pilot exploratory study. *Mov. Disord.* **37**, 2057–2065 (2022).
15. Y. Meng, R. M. Reilly, R. C. Pezo, M. Trudeau, A. Sahgal, A. Singnurkar, J. Perry, S. Myrehaug, C. B. Pople, B. Davidson, M. Llinas, C. Hyen, Y. Huang, C. Hamani, S. Suppiah, K. Hynynen, N. Lipsman, MR-guided focused ultrasound enhances delivery of trastuzumab to Her2-positive brain metastases. *Sci. Transl. Med.* **13**, eabj4011 (2021).
16. Y. Meng, C. B. Pople, Y. Huang, R. M. Jones, J. Ottoy, M. Goubran, L. M. Oliveira, B. Davidson, L. S. P. Lawrence, A. Z. Lau, A. Bethune, P. Maralani, A. Abrahao, C. Hamani, K. Hynynen, S. K. Kalia, N. Lipsman, L. V. Kalia, Putaminal recombinant glucocerebrosidase delivery with magnetic resonance–guided focused ultrasound in Parkinson's disease: A phase I study. *Mov. Disord.* **37**, 2134–2139 (2022).
17. M. E. Karakatsani, J. Blesa, E. E. Konofagou, Blood-brain barrier opening with focused ultrasound in experimental models of Parkinson's disease. *Mov. Disord.* **34**, 1252–1261 (2019).
18. L. Chen, E. Cruz, L. E. Oikari, P. Padmanabhan, J. Song, J. Götz, Opportunities and challenges in delivering biologics for Alzheimer's disease by low-intensity ultrasound. *Adv. Drug Deliv. Rev.* **189**, 114517 (2022).
19. F. Marquet, T. Teichert, S. Y. Wu, Y. S. Tung, M. Downs, S. Wang, C. Chen, V. Ferrera, E. E. Konofagou, Real-time, transcranial monitoring of safe blood-brain barrier opening in non-human primates. *PLOS ONE* **9**, e84310 (2014).
20. S.-Y. Wu, C. Aurup, C. S. Sanchez, J. Grondin, W. Zheng, H. Kamimura, V. P. Ferrera, E. E. Konofagou, Efficient blood-brain barrier opening in primates with neuronavigation-guided ultrasound and real-time acoustic mapping. *Sci. Rep.* **8**, 7978 (2018).
21. M. E. Downs, A. Buch, M. E. Karakatsani, E. E. Konofagou, V. P. Ferrera, Blood-brain barrier opening in behaving non-human primates via focused ultrasound with systemically administered microbubbles. *Sci. Rep.* **5**, 15076 (2015).
22. N. McDannold, C. D. Arvanitis, N. Vykhodtseva, M. S. Livingstone, Temporary disruption of the blood-brain barrier by use of ultrasound and microbubbles: Safety and efficacy evaluation in rhesus macaques. *Cancer Res.* **72**, 3652–3663 (2012).
23. C. Constans, H. Ahnine, M. Santin, S. Lehericy, M. Tanter, P. Pouget, J.-F. Aubry, Non-invasive ultrasonic modulation of visual evoked response by GABA delivery through the blood brain barrier. *J. Control. Release* **318**, 223–231 (2020).
24. D. Goertsen, N. C. Flytzanis, N. Goeden, M. R. Chuapoco, A. Cummins, Y. Y. Chen, Y. Fan, Q. Zhang, J. Sharma, Y. Duan, L. Wang, G. Feng, Y. Y. Chen, N. Y. Ip, J. Pickel, V. Gradinaru, AAV capsid variants with brain-wide transgene expression and decreased liver targeting after intravenous delivery in mouse and marmoset. *Nat. Neurosci.* **25**, 106–115 (2022).
25. Y. Matsuzaki, A. Konno, R. Mochizuki, Y. Shinohara, K. Nitta, Y. Okada, H. Hirai, Intravenous administration of the adeno-associated virus-PHP.B capsid fails to upregulate transduction efficiency in the marmoset brain. *Neurosci. Lett.* **665**, 182–188 (2018).
26. W. A. Liguore, J. S. Domire, D. Button, Y. Wang, B. D. Dufour, S. Srinivasan, J. L. McBride, AAV-PHP.B administration results in a differential pattern of CNS biodistribution in non-human primates compared with mice. *Mol. Ther.* **27**, 2018–2037 (2019).
27. J. Hordeaux, Q. Wang, N. Katz, E. L. Buza, P. Bell, J. M. Wilson, The neurotropic properties of AAV-PHP.B are limited to C57BL/6J mice. *Mol. Ther.* **26**, 664–668 (2018).
28. E. A. Buffalo, J. A. Movshon, R. H. Wurtz, From basic brain research to treating human brain disorders. *Proc. Natl. Acad. Sci. U.S.A.* **116**, 26167–26172 (2019).
29. I. Trigo-Damas, N. L.-G. Del Rey, J. Blesa, Novel models for Parkinson's disease and their impact on future drug discovery. *Expert Opin. Drug Discov.* **13**, 229–239 (2018).
30. J. H. Kordower, C. W. Olanow, H. B. Dodiya, Y. Chu, T. G. Beach, C. H. Adler, G. M. Halliday, R. T. Bartus, Disease duration and the integrity of the nigrostriatal system in Parkinson's disease. *Brain* **136**, 2419–2431 (2013).
31. J. Blesa, G. Foffani, B. Dehay, E. Bezard, J. A. Obeso, Motor and non-motor circuit disturbances in early Parkinson disease: Which happens first? *Nat. Rev. Neurosci.* **23**, 115–128 (2022).
32. G. Foffani, I. Trigo-Damas, J. A. J. A. Pineda-Pardo, J. Blesa, R. Rodríguez-Rojas, R. Martínez-Fernández, J. A. J. A. Obeso, Focused ultrasound in Parkinson's disease: A twofold path toward disease modification. *Mov. Disord.* **34**, 1262–1273 (2019).
33. F. Mingozzi, K. A. High, Immune responses to AAV vectors: Overcoming barriers to successful gene therapy. *Blood* **122**, 23–36 (2013).
34. H. C. Verdera, K. Kuranda, F. Mingozzi, AAV vector immunogenicity in Humans: A long journey to successful gene transfer. *Mol. Ther.* **28**, 723–746 (2020).
35. L. Samaranch, E. A. Salegio, W. San Sebastian, A. P. Kells, K. D. Foust, J. R. Bringas, C. Lamarre, J. Forsayeth, B. K. Kaspar, K. S. Bankiewicz, Adeno-associated virus serotype 9 transduction in the central nervous system of nonhuman primates. *Hum. Gene Ther.* **23**, 382–389 (2012).
36. S. J. Gray, V. Matagne, L. Bachaboina, S. Yadav, S. R. Ojeda, R. J. Samulski, Preclinical differences of intravascular AAV9 delivery to neurons and glia: A comparative study of adult mice and nonhuman primates. *Mol. Ther.* **19**, 1058–1069 (2011).
37. J. J. Vaquero, P. Kinahan, Positron emission tomography: Current challenges and opportunities for technological advances in clinical and preclinical imaging systems. *Annu. Rev. Biomed. Eng.* **17**, 385–414 (2015).
38. A. N. Pouliopoulos, N. Kwon, G. Jensen, A. Meaney, Y. Niimi, M. T. Burgess, R. Ji, A. J. McLuckie, F. A. Munoz, H. A. S. Kamimura, A. F. Teich, V. P. Ferrera, E. E. Konofagou, Safety evaluation of a clinical focused ultrasound system for neuronavigation guided blood-brain barrier opening in non-human primates. *Sci. Rep.* **11**, 15043 (2021).
39. Z. I. Kovacs, S. Kim, N. Jikaria, F. Qureshi, B. Milo, B. K. Lewis, M. Bresler, S. R. Burks, J. A. Frank, Disrupting the blood-brain barrier by focused ultrasound induces sterile inflammation. *Proc. Natl. Acad. Sci. U.S.A.* **114**, E75–E84 (2017).
40. O. Jung, A. Thomas, S. R. Burks, M. L. Dustin, J. A. Frank, M. Ferrer, E. Stride, Neuroinflammation associated with ultrasound-mediated permeabilization of the blood–brain barrier. *Trends Neurosci.* **45**, 459–470 (2022).
41. V. Louis Jeune, J. A. Joergensen, R. J. Hajjar, T. Weber, Pre-existing anti–adeno-associated virus antibodies as a challenge in AAV gene therapy. *Hum. Gene Ther. Methods.* **24**, 59–67 (2013).
42. S. Boutin, V. Monteilhet, P. Veron, C. Leborgne, O. Benveniste, M. F. Montus, C. Masurier, Prevalence of serum IgG and neutralizing factors against adeno-associated virus (AAV) types 1, 2, 5, 6, 8, and 9 in the healthy population: Implications for gene therapy using AAV vectors. *Hum. Gene Ther.* **21**, 704–712 (2010).
43. N. L.-G. del Rey, I. Trigo-Damas, J. A. Obeso, C. Cavada, J. Blesa, Neuron types in the primate striatum: Stereological analysis of projection neurons and interneurons in control and parkinsonian monkeys. *Neuropathol. Appl. Neurobiol.* **48**, e12812 (2022).
44. R. H. Kofoed, C. L. Dibia, K. Noseworthy, K. Xhima, N. Vacaresse, K. Hynynen, I. Aubert, Efficacy of gene delivery to the brain using AAV and ultrasound depends on serotypes and brain areas. *J. Control. Release* **351**, 667–680 (2022).
45. J. R. Mendell, S. Al-Zaidy, R. Shell, W. D. Arnold, L. R. Rodino-Klapac, T. W. Prior, L. Lowes, L. Alfano, K. Berry, K. Church, J. T. Kissel, S. Nagendran, J. L'Italien, D. M. Sproule, C. Wells,

J. A. Cardenas, M. D. Heitzer, A. Kaspar, S. Corcoran, L. Braun, S. Likhite, C. Miranda, K. Meyer, K. D. Foust, A. H. M. Burghes, B. K. Kaspar, Single-dose gene-replacement therapy for spinal muscular atrophy. *N. Engl. J. Med.* **377**, 1713–1722 (2017).

46. R. Vali, W. Loidl, C. Pirich, W. Langesteger, M. Beheshti, Imaging of prostate cancer with PET/CT using ^{18}F-Fluorocholine. *Am. J. Nucl. Med. Mol. Imaging* **5**, 96–108 (2015).
47. T. R. DeGrado, S. W. Baldwin, S. Wang, M. D. Orr, R. P. Liao, H. S. Friedman, R. Reiman, D. T. Price, R. E. Coleman, Synthesis and evaluation of (18)F-labeled choline analogs as oncologic PET tracers. *J. Nucl. Med.* **42**, 1805–1814 (2001).
48. W. M. Arif, P. H. Elsinga, C. Gasca-Salas, M. Versluis, R. Martínez-Fernández, R. A. J. O. Dierckx, R. J. H. Borra, G. Luurtsema, Focused ultrasound for opening blood-brain barrier and drug delivery monitored with positron emission tomography. *J. Control. Release* **324**, 303–316 (2020).
49. G. Hugon, S. Goutal, A. Dauba, L. Breuil, B. Larrat, A. Winkeler, A. Novell, N. Tournier, [^{18}F]2-Fluoro-2-deoxy-sorbitol PET imaging for quantitative monitoring of enhanced blood-brain barrier permeability induced by focused ultrasound. *Pharmaceutics* **13**, 1752 (2021).
50. P. A. LeWitt, A. R. Rezai, M. A. Leehey, S. G. Ojemann, A. W. Flaherty, E. N. Eskandar, S. K. Kostyk, K. Thomas, A. Sarkar, M. S. Siddiqui, S. B. Tatter, J. M. Schwalb, K. L. Poston, J. M. Henderson, R. M. Kurlan, I. H. Richard, L. Van Meter, C. V. Sapan, M. J. During, M. G. Kaplitt, A. Feigin, AAV2-GAD gene therapy for advanced Parkinson's disease: A double-blind, sham-surgery controlled, randomised trial. *Lancet Neurol.* **10**, 309–319 (2011).
51. J. Blesa, C. Pifl, M. A. Sánchez-González, C. Juri, M. A. García-Cabezas, R. Adánez, E. Iglesias, M. Collantes, I. Peñuelas, J. J. Sánchez-Hernández, M. C. Rodríguez-Oroz, C. Avendaño, O. Hornykiewicz, C. Cavada, J. A. Obeso, The nigrostriatal system in the presymptomatic and symptomatic stages in the MPTP monkey model: A PET, histological and biochemical study. *Neurobiol. Dis.* **48**, 79–91 (2012).
52. K. Y. Chan, M. J. Jang, B. B. Yoo, A. Greenbaum, N. Ravi, W. L. Wu, L. Sánchez-Guardado, C. Lois, S. K. Mazmanian, B. E. Deverman, V. Gradinaru, Engineered AAVs for efficient noninvasive gene delivery to the central and peripheral nervous systems. *Nat. Neurosci.* **20**, 1172–1179 (2017).
53. K.-I. Inoue, R. Kimura, N. Yasukochi, M. Okuda, M. Fujiwara, M. Takada, "Intravascular administration of an AAV vector to neonatal macaques results in widespread gene transduction into neurons throughout the primate braintle" in *Society for Neuroscience 2014* (Washington, DC, USA, 2014), p. 657.10/UU75.
54. A. K. Bevan, S. Duque, K. D. Foust, P. R. Morales, L. Braun, L. Schmelzer, C. M. Chan, M. McCrate, L. G. Chicoine, B. D. Coley, P. N. Porensky, S. J. Kolb, J. R. Mendell, A. H. M. Burghes, B. K. Kaspar, Systemic gene delivery in large species for targeting spinal cord, brain, and peripheral tissues for pediatric disorders. *Mol. Ther.* **19**, 1971–1980 (2011).
55. M. Moskalenko, L. Chen, M. van Roey, B. A. Donahue, R. O. Snyder, J. G. McArthur, S. D. Patel, Epitope mapping of human anti-adeno-associated virus type 2 neutralizing antibodies: Implications for gene therapy and virus structure. *J. Virol.* **74**, 1761–1766 (2000).
56. A. Meliani, C. Leborgne, S. Triffault, L. Jeanson-Leh, P. Veron, F. Mingozzi, Determination of anti-adeno-associated virus vector neutralizing antibody titer with an *in vitro* reporter system. *Hum. Gene Ther. Methods.* **26**, 45–53 (2015).
57. M. J. West, Stereological methods for estimating the total number of neurons and synapses: Issues of precision and bias. *Trends Neurosci.* **22**, 51–61 (1999).
58. D. H. Paulus, H. H. Quick, C. Geppert, M. Fenchel, Y. Zhan, G. Hermosillo, D. Faul, F. Boada, K. P. Friedman, T. Koesters, Whole-body PET/MR imaging: Quantitative evaluation of a novel model-based mr attenuation correction method including bone. *J. Nucl. Med.* **56**, 1061–1066 (2015).

Acknowledgments: We are grateful to V. Soler (Medical Director), L. Díaz-Jiménez Fernandez, M. Lorca-Moreno, and S. Casas from the Radiology Department and U. Alcañas Martínez and Y. Gomez Gonzalez of the Nuclear Medicine Department in HM Puerta del Sur Hospital. We thank J. H. Kordower and J. F. Aubry for helpful discussions and insightful comments on the manuscript. We thank L. Phillips, MD for English language editing of this manuscript. **Funding:** This work was supported by Ministerio de Ciencia e Innovación y Universidades (PID2019-111045RB-I00) (J.A.O.), (PID2021-127800OA-I00) (J.A.P.-P.), and (IJC2020 -043918-I) (T.B.); Instituto de Salud Carlos III Miguel Servet (MS19/00200) and FIS (PI20/00496) (J.B.) and PFIS (FI21/000919) (N.E.-G.); Fundación Tatiana Pérez de Guzmán el Bueno (J.B.); Grant-in-Aid for Scientific Research from Japan Society for the Promotion of Science (no. 19H05467 to M.T. and 22H05157 and 22 K19480 to K.I.); Japan Agency for Medical Research and Development (JP19dm0207077 to M.T.); Focused Ultrasound Foundation; Fundación MAPFRE; Fundación BBVA; and a joint project between Fundación de Investigación HM Hospitales and Insightec Ltd. **Author contributions:** Conceptualization: J.B., J.A.P.-P., C.G.-S., and J.A.O. Methodology: J.B., J.A.P.-P., K.I., C.G.-S., T.B., N.L.-G.R., A.R.-S., N.E.-G., R.R.-R., R.M., M.C., M.A., L.G.-C., S.R.A., I.T.-D., I.R., and M.T. Funding acquisition: J.B., J.A.P.-P., K.I., M.T., and J.A.O. Writing—original draft: J.B., J.A.P.-P., K.I., T.B., M.T., and J.A.O. Writing—review and editing: All authors read and approved the final version. **Competing interests:** I.R. is an employee of Insightec Ltd. that developed and commercializes the focused ultrasound transducer used in this study. J.A.O. has been a member of the Advisory Board of Insightec Ltd. (2021–2022). The authors declare that they have no other competing interests. **Data and materials availability:** All data needed to evaluate the conclusions in the paper are present in the paper and/or the Supplementary Materials.

Submitted 25 October 2022
Accepted 20 March 2023
Published 19 April 2023
10.1126/sciadv.adf4888

ScienceAdvances

BBB opening with focused ultrasound in nonhuman primates and Parkinson's disease patients: Targeted AAV vector delivery and PET imaging

Javier Blesa, Jos A. Pineda-Pardo, Ken-ichi Inoue, Carmen Gasca-Salas, Tiziano Balzano, Natalia Lpez-Gonzlez Del Rey, Alejandro Reinares-Sebastin, Noelia Esteban-Garca, Rafael Rodrguez-Rojas, Raquel Mrquez, Mara Ciorraga, Marta del lamo, Lina Garca-Caamaque, Santiago Ruiz de Aguiar, Itay Rachmilevitch, Ins Trigo-Damas, Masahiko Takada, and Jos A. Obeso

Sci. Adv., **9** (16), eadf4888.
DOI: 10.1126/sciadv.adf4888

Science Advances (ISSN) is published by the American Association for the Advancement of Science. 1200 New York Avenue NW, Washington, DC 20005. The title *Science Advances* is a registered trademark of AAAS.